

AD

AD-E402 791

Technical Report ARAED-TR-96014

**CONCRETE PENETRATION BY ERODING PROJECTILES:  
EXPERIMENTS AND ANALYSIS**

Vladimir M. Gold

December 1996



US ARMY  
TANK AUTOMOTIVE AND  
ARMAMENTS COMMAND  
ARMAMENT RDE CENTER

**U.S. ARMY ARMAMENT RESEARCH, DEVELOPMENT AND  
ENGINEERING CENTER**

Armament Engineering Directorate

**Picatinny Arsenal, New Jersey**

Approved for public release; distribution is unlimited.

DTIC QUALITY INSPECTED 4

19970116 061

The views, opinions, and/or findings contained in this report are those of the authors(s) and should not be construed as an official Department of the Army position, policy, or decision, unless so designated by other documentation.

The citation in this report of the names of commercial firms or commercially available products or services does not constitute official endorsement by or approval of the U.S. Government.

Destroy this report when no longer needed by any method that will prevent disclosure of its contents or reconstruction of the document. Do not return to the originator.

## REPORT DOCUMENT PAGE

Form Approved  
OMB No. 0704-0188

Public reporting burden for this collection of information is estimated to average 1 hour per response, including the time for reviewing instruction, searching existing data sources, gathering and maintaining the data needed, and completing and reviewing the collection of information. Send comments regarding this burden estimate or any other aspect of this collection of information, including suggestions for reducing this burden, to Washington Headquarters Services, Directorate for Information Operations and Reports, 12115 Jefferson Davis Highway, Suite 1204, Arlington, VA 22202-4302, and to the Office of Management and Budget, Paperwork Reduction Project (0704-0188), Washington, DC 20503.

1. AGENCY USE ONLY (Leave blank)

2. REPORT DATE

December 1996

3. REPORT TYPE AND DATES COVERED

Final

4. TITLE AND SUBTITLE

CONCRETE PENETRATION BY ERODING PROJECTILES:  
EXPERIMENTS AND ANALYSIS

5. FUNDING NUMBERS

PAM PE 604040

A3 PE 622618

Target Defect

PE 622624

6. AUTHOR(S)

Vladimir M. Gold

7. PERFORMING ORGANIZATION NAME(S) AND ADDRESS(ES)

ARDEC, AED

Energetics and Warheads Division (AMSTA-AR-AEE-W)

Picatinny Arsenal, NJ 07806-5000

8. PERFORMING ORGANIZATION  
REPORT NUMBER

9. SPONSORING/MONITORING AGENCY NAME(S) AND ADDRESS(ES)

ARDEC, LSED

Information Research Center (AMSTA-AR-LSL)

Picatinny Arsenal, NJ 07806-5000

10. SPONSORING/MONITORING  
AGENCY REPORT NUMBER

11. SUPPLEMENTARY NOTES

12a. DISTRIBUTION/AVAILABILITY STATEMENT

Approved for public release; distribution is unlimited.

12b. DISTRIBUTION CODE

13. ABSTRACT (Maximum 200 words)

Spherical-nose copper and tantalum rods with aspect ratios between 4.0 and 14.6 were gun launched against 91-cm dia and 91-cm long concrete and simulant reinforced concrete targets with velocities ranging from 0.15 cm/ $\mu$ s to 0.19 cm/ $\mu$ s. Targets were instrumented with a sequence of break gages which provided valuable data for characterizing the penetration process. Target hole profiles and projectile residual masses were measured and reported. Analysis of the penetration performance of projectiles was performed within the framework of the modified hydrodynamic theory of penetration. Based on the results of these calculations, the penetration efficiencies of the copper and the tantalum projectiles are compared as functions of impact velocities. Analysis of the penetration resistance of the simulant reinforced concrete targets was based on treating the targets as "composites", comprised of layers of concrete proper and reinforcing steel; the results of these calculations are compared with the experimental data. Using this theory, the penetration resistance of a concrete/steel/concrete "composite" is investigated as a function of the following parameters: thickness of the surface layer of the concrete, thickness of the steel reinforcement, and impact velocity.

14. SUBJECT TERMS

Concrete instrumentation

Concrete target

Projectile

Modified hydrodynamic

Theory of penetration

Plastic zone

15. NUMBER OF PAGES 33

16. PRICE CODE

17. SECURITY CLASSIFICATION  
OF REPORT

UNCLASSIFIED

18. SECURITY CLASSIFICATION  
OF THIS PAGE

UNCLASSIFIED

19. SECURITY CLASSIFICATION  
OF ABSTRACT

UNCLASSIFIED

20. LIMITATION OF ABSTRACT

SAR

## CONTENTS

	Page
Introduction	1
Experiments	3
Analysis of the Impact Resistance of Concrete and Reinforced Concrete Targets	6
Conclusions	10
References	25
Distribution List	29

## FIGURES

		Page
1.	Schematic of experimental setup	11
2.	Plain concrete target after impact	12
3.	Simulant reinforced concrete target after impact	13
4.	Rod with initial velocity $v_0$ impacts a composite semi-infinite targets	14
5.	Normalized penetration depth vs impact velocities	15
6.	Calculated penetration performance of copper and tantalum projectiles against plain concrete targets compared with experimental data for varying impact velocities	16
7.	Calculated trajectories of front end of projectile compared with experimental records from break gages - plain concrete	17
8.	Calculated trajectories of front end of projectiles compared with experimental records from break gages - simulant reinforced concrete, $v_0 = 0.1875 \text{ cm}/\mu\text{s}$	18
9.	Resistance of a concrete/steel/concrete composite vs the thickness of the surface layer of concrete	19
10.	Penetration resistance, areal weight, and areal cost of a concrete/steel/concrete composite structure vs the thickness of the steel layer	20
11.	Penetration performance of a tantalum projectile against a concrete/steel/concrete composite with different thickness' of the steel layer vs the impact velocity	21

## TABLES

### Page

1. Performance of copper (Cu) and tantalum (Ta) projectiles  
against plain concrete targets (PC) and simulant reinforced  
concrete targets (RC)
2. Hole profiles of tunnel portions of craters

23

23

## SYMBOLS AND ABBREVIATIONS

Notation	Definition
$D$	diameter of the penetrator
$h$	thickness of the steel layer
$l$	instantaneous length of the penetrator
$L$	initial length of the penetrator
$p$	instantaneous penetration depth
$P$	the depth of penetration
$R$	strength factor of the target
$R_i$	strength factor of the $i^{\text{th}}$ layer of the target
$\tau$	time
$T_i - 0$ and $T_i + 0$	time the penetrator exiting the $i^{\text{th}}$ layer and entering the $(i + 1)^{\text{st}}$ layer of the target, respectively
$u$	penetration rate
$v$	velocity of the rigid portion of the penetrator
$v_0$	projectile impact velocity
$Y$	strength factor of the penetrator
$z_i$	position of an interface between $i^{\text{th}}$ and $(i + 1)^{\text{st}}$ layer of a composite target
$\rho_p$ and $\rho_t$	densities of the penetrator and the target, respectively
$\rho_i$	density of the $i^{\text{th}}$ layer of the target
$w$	areal weight of a structure
$\Omega$ , $\Omega_c$ and $\Omega_r$	areal costs per unit depth of the structure for: reinforced concrete, plain concrete, and reinforcing steel, respectively

## INTRODUCTION

The subject of the penetration and perforation of concrete has long been of interest in the military field and recently commanded attention in a number of other applications including the design of impact resistant structures for nuclear power plants, various industrial buildings, hardened protective facilities, etc. A review of previous work shows that extensive concrete penetration studies were performed in the early 1940's. However, most of this work ceased shortly after World War II and was not resumed until the 1960's.

Depending on a number of factors, such as the relative size and strength of the projectile and the target, the impact velocity, etc., the penetration can cease with or without the projectile exiting the target. The penetration mode that is associated with the complete piercing through the thickness of the target, usually referred to as target perforation, has been extensively investigated by many researchers. A collection of concrete slab perforation data can be found in Nash *et al* (ref 1).

Because of the absence of the rear surface, semi-infinite target penetration provides conditions that are nearly ideal for penetration resistance studies. When a projectile penetrates a semi-infinite body of concrete, it continuously crushes the material in front of it and pushes it out radially. Under the pressure exerted at the interface between the projectile and the target, the penetrator front can deform into a characteristic mushroom-like shape, the extent of this deformation varying significantly with the impact velocity and the relative strength of the projectile and the target. A combination of all these factors determines a target's penetration resistance.

For relatively low impact velocities (typically, below  $0.1 \text{ cm}/\mu\text{s}$ ) the penetrator remains virtually undeformed. For this range of the impact velocities, high strength grades of steel are usually employed for the penetrator material, and the available experimental data (refs 1 through 5) show nearly linear increases in the penetration depth with increases in impact velocity. Given that the penetrator is rigid, and assuming that the analytical expression for the penetration resistance force is known, the analysis of the penetrator motion is rather straight forward. Most of these analytical techniques rely either on various empirical formulations (refs 6 through 8) or employ a more rigorous approach based on the cavity-expansion approximations (refs 9 and 10).

With increases in the impact velocity, the penetrator front starts to "mushroom" leading to the erosion of the penetrator which significantly degrades its penetration performance. Only a limited amount of experimental data for concrete is reported in the literature for impact velocities above  $0.1 \text{ cm}/\mu\text{s}$ . Experiments with tungsten (ref 11) and tantalum (ref 12) penetrators show that for velocities in the range of  $0.39 \text{ cm}/\mu\text{s}$  to  $0.46 \text{ cm}/\mu\text{s}$  the concrete penetration depths are proportional to the penetrator's loss of length, which is in a close agreement with the ideal hydrodynamic theory of penetration (ref 13). Miller and McKay (ref 14) experimented with tungsten penetrators in a much wider range of velocities from  $0.09 \text{ cm}/\mu\text{s}$  to  $0.43 \text{ cm}/\mu\text{s}$  using a reverse ballistics technique (i.e.,



small concrete targets were launched against stationary penetrators). Although the reported data are scattered, they still show a reasonable agreement with the hydrodynamic theory at the higher range of the impact velocities tested. The limited number of experiments reported for the lower range of impact velocities (below  $0.2 \text{ cm}/\mu\text{s}$ ), show a significant decrease in the target bore hole diameters. This indicates a decrease in the extent of penetrator deformation and transition to the "rigid body" lower velocity penetration mode.

The experiments presented in this work pertain to the penetration performance of copper and tantalum projectiles with velocities from  $0.15 \text{ cm}/\mu\text{s}$  to  $0.19 \text{ cm}/\mu\text{s}$ . At these velocities, while the penetrator can undergo significant deformation and erosion, the impact velocities are still not high enough to ignore the strength of the target and penetrator materials. In this velocity range, analysis of the penetration can be carried out using a modified (i.e., strength dependent) hydrodynamic theory of penetration (refs 15 and 16). Employment of this theory requires knowledge of two empirical constants that are usually referred to as the projectile and the target dynamic strength factors  $Y$  and  $R$ , respectively. Once the values of these constants are determined through an experiment, the theory can be used to predict the penetration resistance of various concrete and steel reinforced concrete structures for a wide range of impact velocities.

Another important aspect of the present work is the acquisition of the penetration history data in concrete using a sequence of break gages. When a penetrator moves in a target supersonically, the break gage trigger time (i.e., the time of the gage rupture) coincides with the penetrator's arrival at the gage. Thus, the sequence of the trigger times of gages which are placed at the designated positions in the target, allows the exact determination of the rate of penetration. This technique was originally introduced by Eichelberger (ref 17) for shape charge jets penetrating stacks of metal plates, and later was applied to sand targets by Allen *et al* (ref 18). A variety of techniques for the acquisition of the penetration history data in metallic targets were developed by Weihrauch and Lehr (ref 19) and Weihrauch (ref 20). Employment of the penetration rate break gage measurement technique at subsonic velocities for laminated and predrilled metallic targets is reported by Netherwood (ref 21) designing the experiments presented in this work, the break gage measurement technique was applied for concrete and reinforced concrete targets penetrated at subsonic velocities. When the penetrator moves within the target subsonically, the break gage trigger time indicates the instant of the fracturing of concrete at the gage location, occurring some distance ahead of the penetrator. Thus, in the case when the target penetration rate is below the sonic velocity, the sequence of the break gage trigger times determine the evolution of the boundary of the plastic zone ahead of the penetrator, rather than the trajectory of the front of the penetrator itself.

Numerous experimental and analytical studies of penetration with high aspect ratio ( $L/D$ ) projectiles indicate that the trajectory of the front end of the penetrator consists of two distinct regions: a long region of approximately steady state penetration and a short deceleration. The technique for determining the extent of the plastic zone in front of the

penetrator, introduced in this work, is based on the fact that the projectile penetration rate in the steady state region depends strongly on the impact velocity and the densities of the projectile and the target, and only weakly on their strengths. This allows an accurate prediction of this region of the penetrator trajectory without a detailed knowledge of the constitutive behavior of the target material. Thus, when break gages are placed in the region of the steady state penetration, the size of the plastic zone in front of the penetrator can be determined as the difference between the experimentally established trajectory of the elastic-plastic front (based on the break gage trigger times) and the calculated trajectory of the penetrator. This provides unique data for characterizing the penetration process, and further discussion on this technique can be found later in the paper.

## EXPERIMENTS

Terminal ballistic experiments were conducted to establish the resistance of semi-infinite concrete and reinforced concrete structures attacked by high velocity projectiles. Spherical-nose cylindrical copper and tantalum projectiles, with 1.3-cm and 2.0-cm diameters and varying length to diameter ratios ( $L/D$ ), were gun launched against simulant concrete and reinforced concrete targets with the velocities ranging from 0.15 cm/ $\mu$ s to 0.19 cm/ $\mu$ s. All but two of the targets were instrumented with evenly spaced break gages, and as the projectile penetrated the target the trigger times of these gages were recorded.

The simulant targets were 91-cm diameter and 91-cm long right circular cylinders, and were constructed from a concrete with maximum aggregate size of 1.9 cm. The concrete was poured approximately 35 days prior to the ballistic experiments, and 10 specimens of that concrete were taken for strength tests. The compressive strength tests conducted on the 28<sup>th</sup>, 46<sup>th</sup>, and 49<sup>th</sup> days of cure, gave an average unconfined strength of 0.374 Kbar.

When concrete is impacted by a high velocity projectile it is prone to shatter. For instance, Krause *et al.* (ref 11) report a complete destruction of 61- x 61- x 61-cm unconstrained concrete and reinforced concrete targets that were impacted with velocities about 0.45 cm/ $\mu$ s. In order to minimize the influence of the lateral boundary of these moderately sized targets (i.e., to prevent their shattering and to achieve accurate hole profiles), the lateral surface was constrained by a spiral reinforcing bar and tack welded to the enclosing corrugated steel shell. The rear and front ends of the skeleton of this structure were also fortified by a grid of transverse reinforcing bars, and the rear end grid was tack welded to a thin steel end plate. Since the diameter of the structure exceeded the projectile diameters by 50 to 70 times and the lateral and rear boundaries were heavily constrained, only local deformations (compared to the size of the target) were expected at the impact site. Although the resulting penetration depths were of the order of one-third to one-half of the length of the targets, no visible traces of deformation were found in the rear of the structures. The examination of the condition of concrete near the edge of the front surface indicated that this portion of the material was subjected to a relatively low strain

field. This further supported our initial assumption that the size of the targets would be adequate in approximating the impact response of a semi-infinite configuration.

The targets that were intended to simulate the impact response of semi-infinite reinforced concrete, included a 1.6-cm thick and 30.5-cm square steel plate imitating a reinforced rebar, which was embedded 3.8 cm away from the front face of the target and welded to the front grid of the transverse reinforcing bars. The probability of hitting 1.6 cm rebar by a gun launched projectile is very low, and this was the reason for simulating the reinforcing rebar with a steel plate of an equal thickness and strength. Steel grades with similar strength characteristics were used for both the plates and the reinforcing bars, which according to the manufacturer's specifications had a yield strength of 4.1 Kbar.

Eight targets were instrumented with break gages, which enabled observing the evolution of the elastic-plastic front during the penetration. The break gages were 14-cm by 26-cm and 0.33-mm thick rectangular printed circuit boards. They consisted of two conductive copper foils enclosing an insulated copper foil maze between them. When the gage is being operated, a voltage is applied to the gage and monitored for sudden interruptions, which are directly associated with either breaking the maze foil or with making a contact between one of the outer foils and the maze. Thus, when the gage is subjected to severe deformation sufficient to break it, the interruption in the applied voltage registers the time of that event. Seven break gages were placed in a form and carefully positioned starting 2.54 cm from the reference edge of the form and 2.54 cm apart for each other. After the pouring and curing of the concrete, the 8<sup>th</sup> gage was positioned onto the reference edge of this block, and the concrete block containing all the break gages were placed inside the target skeleton and the target was poured. When pouring the simulant reinforced concrete targets, the block containing the break gages was placed flush to the rear of the plate, and the additional 9<sup>th</sup> gage was attached to the front surface of the plate. For the plain concrete targets the block was positioned 5.4 cm away from the front face of the target. At the time of the experiments an additional break gage was taped to the front face of the target. This gage was used as a reference to register the time of the impact of the projectile, and the break times of the subsequent gages were counted relative to this time. Immediately prior to the ballistic tests, the electrical resistance of the gages was examined, and only a few gages were found to be defective. The data from these gages were ignored.

The schematic of the test set up is shown in figure 1. The projectiles were positioned in a plastic sabot, placed in a 83-mm diameter and 10.9-m long launching tube, and fired. To ensure the structural integrity of the projectile-sabot assembly during the rapid acceleration in the launching tube, the rear end of the sabot was reinforced with an aluminum pusher plate. At the downstream end of the launching tube, past the gas expansion chamber, the accelerated projectile followed by the separating sabot proceeded along the drift tube, where their motion was photographed at two orthogonal viewing stations with a streak camera. The states were 75 cm apart for each other, and comparing the two photographs taken at the set exposure times provided reliable measurement of the

projectile's velocity. The targets rested under their own weight on a wooden platform and the entire assembly was housed in a massive steel tank. The access for the two x-ray shadowgraph systems was provided through the horizontal and vertical window ports located at the side wall of the steel tank. The x-rays were focused to cover the area in front of the target, so that the yaw and the condition of the projectile just prior to the impact was confidently established from the shadowgraphs. The targets were positioned approximately 1 m away for the muzzle of the gun, however, this distance was insufficient for complete aerodynamic separation of the sabot. In order to minimize the damage to the front of the target by the debris of the sabot assembly, a sandwich of plywood and steel plates with a circular opening along the path of the projectile, was placed directly onto the target's surface. The diameter of the hole and the thickness of this buffer were selected so as to allow the projectile to freely pass through them, while stopping the aluminum pusher plate and the sabot parts from reaching the target. Two break screens placed 30.5 cm apart for each other were employed to trigger the x-ray system as well as to provide an auxiliary measurement of the projectile velocity. The impact velocities were also verified from the x-rays, which correlated well with streak camera records.

The projectiles were launched with velocities ranging from 0.15 cm/ $\mu$ s to 0.19 cm/ $\mu$ s. The performance of the projectiles is summarized in table 1, while the typical post impact condition of the plain and simulant reinforced concrete targets is shown in figures 2 and 3. An impact onto a plain concrete target resulted in an approximately 25-cm diameter crater at the face, rapidly narrowing down to a diameter of 5-cm at a depth of 10.5-cm away from the original face of the target. The deeper portion of the crater was very well preserved and had the distinct form of a well rounded and slightly tapered tunnel. For the simulant reinforced concrete targets, the form of the entrance of the crater was significantly perturbed, since the front layer of the concrete was shaken off by the motion of the steel plate being exited by the projectile piercing the plate. For example, in test PA9Cu1.1 (fig. 3) the welds holding the plate failed and the plate was thrown out for then target. Behind the plate, the hole was very well preserved, and similarly to the plain concrete targets, it resembled a well rounded and slightly tapered tunnel. The profiles of the tunnel portions of the craters are given in table 2. The front surfaces of all the targets exhibited characteristic radial cracks originating at the center and propagating outwardly. Thus, the caution taken in providing an elaborate reinforcement of the lateral boundary of these moderately sized targets did pay off, and the targets retained their structural integrity after the impact.

All the targets were sectioned and searched for residual parts of the projectiles. The results of this sectioning are given in table 1. No evidence of projectile material in the crater was reported for the tests PA9Cu.1, PA0Cu2.RL10, and for all but one of the tests with tantalum projectiles. Careful examination of the other targets indicated presence of debris which were deposited at the bottom of the tunnel. The two targets impacted with 14-cm long, 1.3-cm diameter projectiles (with initial weight of 164 g) contained only 25 g and 54 g of debris, while the rest of the projectile's material was apparently eroded during the penetration. Since all the experiments show that the penetration was accompanied by either significant or almost complete projectile erosion, the penetration analysis can be

carried out using hydrodynamic approximations (i.e., either ideal or strength corrected). In the test with more massive projectiles (PA8Cu1.4 and PA9Cu3.5) the projectile remains weighed as much as 40 to 50% of their initial weight, meaning that the penetration did not end because of the complete projectile erosion by rather due to the penetrator's deceleration. Thus, for the analysis of the penetrator motion it is appropriate to use modified hydrodynamic approximations which take into consideration effects related to the strengths of the projectile and the target.

## ANALYSIS OF THE IMPACT RESISTANCE OF CONCRETE AND REINFORCED CONCRETE TARGETS

The one-dimensional modified (i.e., strength dependent) hydrodynamic theory of penetration (ref 16 and 22) can be applied to interpret the experimental results and to predict the penetration resistance of various concrete structures. Within the framework of this theory, the essence of the mechanics of penetration of a solid projectile into a solid target is represented though erosion of the penetrator material which is combined with its rigid body motion. Although, the theory neglects the three-dimensional nature of the flow field of the interacting projectile and target, it still demonstrates good qualitative and quantitative agreement of the impact velocities in the ballistic range (ref 23).

The model presumes that the projectile is rigid, except for a thin region near the interface between the target and the projectile where erosion is occurring. This region has no spatial extent and contains only the interface between the target and the projectile. The rate of the projectile erosion is controlled by the pressure at the interface which is give by

$$\frac{1}{2}\rho_p(u-v)^2 + Y = \frac{1}{2}\rho_t u^2 = R \quad (1)$$

In this equation  $\rho_p$  and  $\rho_t$  are the projectile and target densities, respectively,  $v$  is the speed of the rigid portion of the projectile,  $u$  is the penetration rate (or the velocity of the interface between the projectile and the target), and  $Y$  and  $R$  are the strength of the projectile and the target, respectively. In this model  $Y$  and  $R$  are the only empirical constants which have to be determined experimentally for each combination of projectile and target materials.

The rigid portion of the penetrator is decelerated by the axial force exerted by the eroding portion. Since the maximum stress that the penetrator can sustain is  $Y$ , the deceleration is given by:

$$Y = -\rho_p l \frac{dv}{dt} \quad (2)$$

where  $l$  is the current length of the penetrator. The rate of erosion of the penetrator is given by:

$$\frac{dl}{dt} = -(v - u) \quad (3)$$

A rationale for treating the reinforced concrete targets as comprised of layers of concrete proper and reinforcing steel was adopted (fig. 4). With this approach, the increased resistance of the reinforced concrete is primarily attributed to the properties (strength and density) and the thickness of the reinforcing element, while the intricate effects of interactions between the penetrator, the reinforcing steel, and the concrete are neglected. Thus, the motion of a projectile penetrating a "composite" target is governed by the set of equations 1 to 3 which are sequentially applied to each of the layers:

$$\begin{aligned} Y &= -\rho_p l \frac{dv}{dt} \\ \frac{dl}{dt} &= -(v - u) \\ \frac{1}{2} \rho_p (u - v)^2 + Y &= \frac{1}{2} \rho_i u^2 + R_i \end{aligned} \quad (4)$$

Here,  $\rho_i$  and  $R_i$  are, respectively, the density and the strength of the  $i^{\text{th}}$  layer of the target (e.g., for plain concrete,  $i = 1$ ; for reinforced concrete  $i = 1, 2, 3$ ). The initial conditions are

$$\begin{aligned} l(t=0) &= L \\ v(t=0) &= v_0 \end{aligned} \quad (5)$$

where  $L$  and  $v_0$  are the penetrator's initial length and velocity, respectively. When the penetrator crosses the  $i^{\text{th}}$  interface, the conditions of continuity take the same form as the initial conditions for the  $(i + 1)^{\text{st}}$  layer, i.e.,

$$\begin{aligned} l(T_i + 0) &= l(T_i - 0) \\ v(T_i + 0) &= v(T_i - 0) \end{aligned} \quad (6)$$

where  $T_i - 0$  and  $T_i + 0$  refer to the times that the projectile is exiting from the  $i^{\text{th}}$  layer and entering the  $(i + 1)^{\text{st}}$ , respectively. Since the penetration rate  $u$  is a function of the target material in each layer, the penetration rate need not be continuous at the layer interfaces, i.e., in general,  $u(T_i + 0) \neq u(T_i - 0)$ . For instance, for the target shown in figure 4, when the penetrator enters the steel, the penetration rate is decreased,  $u(T_i + 0) < u(T_i - 0)$ ; while when it exits the steel and enters the concrete, the penetration rate is increased,  $u(T_i + 0) > u(T_i - 0)$ .

The system of equation 4 was integrated numerically and the normalized penetration  $P\mu/L$ , where  $P$  is the penetration depth and  $\mu^2 = \rho_t/\rho_p$ , was computed as a function of the initial impact velocity  $v_0$  for various values of the strength factors  $R$  and  $Y$ . Plots of these curves are shown in figure 5. The constants  $R$  and  $Y$  affect the shape of the curves quite differently. Penetration of low velocity projectiles is governed by  $R$  and is quite insensitive to  $Y$ . The opposite is true in the case of impact velocities in the region that corresponds to the maximum penetration depth. For very high impact velocities,  $P$  attains an asymptotic value independent of  $R$  and  $Y$ . The shape of the curves is very sensitive to changes in  $R$  and  $Y$ ; increases in the value of target strength  $R$  decrease the slopes of the curves in the lower velocity region, while increase in the penetrator strength  $Y$  shift the curves along the slopes (determined by  $R$ ) and increase penetration depths. The values of the empirical constant  $R$  and  $Y$  can be determined by comparisons of these curves with the available experimental data.

Figure 6 shows curves of the penetration depth per areal mass of the penetrator  $P/L\rho_p = f(v_0)$  for both the copper and the tantalum projectiles. Such a normalization allows to collate and compare the penetration capabilities of projectiles of different materials and the same kinetic energy. Comparison the these curves can be useful for determining relative penetration efficiencies of different materials.

The set of values  $R = 4.26$  Kbar for concrete,  $Y = 6.86$  Kbar for copper, and  $Y = 13.44$  Kbar for tantalum seems to provide the best agreement with the low velocity data for steel projectiles, as reported by Canfield (ref 3), as well and with the copper and tantalum data from this work. The values of  $Y = 6.86$  Kbar and  $Y = 13.44$  Kbar compare with the respective values of copper and tantalum of  $Y = 3.8$  Kbar and  $Y = 11.0$  Kbar found by Wilkins and Guinan (ref 24) at much lower velocities. The difference in the values of copper is 75%, while for tantalum is 22%, and these variations may be attributed to rate and thermal effects as well as the initial condition of the stock material.

Comparing the calculated curves for copper and tantalum projectiles, tantalum is estimated to be a more efficient penetrator material than copper for the lower velocities, while the reverse is true for the higher velocities. Since the dynamic strengths of these metals (and, in fact, of most of the metals) exceed the strength of concrete, penetration mode combining rigid body motion and erosion is possible. Therefore, there may exist an optimum velocity at which the penetration depth is maximized. According to the modified hydrodynamic theory of penetration, in the lower velocity region the penetration is dominated by the penetrator's rigid body motion. Decreases in the projectile strength  $Y$  increase the penetrator erosion which in turn decreases overall penetration performance.

The instantaneous penetration  $p = p(v)$  and the corresponding time  $t = t(v)$  were computed by solving the system of equation 4. These two functions represent a trajectory of the front end of a projectile, where the parameter  $v$  is the velocity of the rear end of the projectile,  $0 \leq v \leq v_0$ . In figures 7 and 8 we compared the results of these calculations with the experimental trigger time data from the break gages. For the plain concrete (fig. 7),

while the slope of the experimental data curve agrees very well with the slope of the calculated trajectory of the projectile, there is a significant offset between the curves. This offset can be attributed to the early trigger times of the break gages ahead of the projectile, apparently at the elastic-plastic boundary, where the strains are sufficient to cause an interruption in the applied voltage. Similar is the situation with the simulant reinforced concrete (fig. 8), where the calculated trajectory exhibits a distinct change of slope (or penetration rate)  $u = dp/dt$  as the projectile enters and exits different material layers of the target, and a similar trend can be detected in the experimental data.

Figure 9 presents the results of penetration calculations for a "composite" concrete/steel/concrete target as a function of the thickness of the first layer of concrete, while the thickness of the steel layer remains constant. The analysis shows virtually identical penetrations for almost the entire range of the calculations. Since the computational model completely ignores the details of the flow field of the penetrator and the target materials, these calculations might not be realistic for small thickness of the first layer.

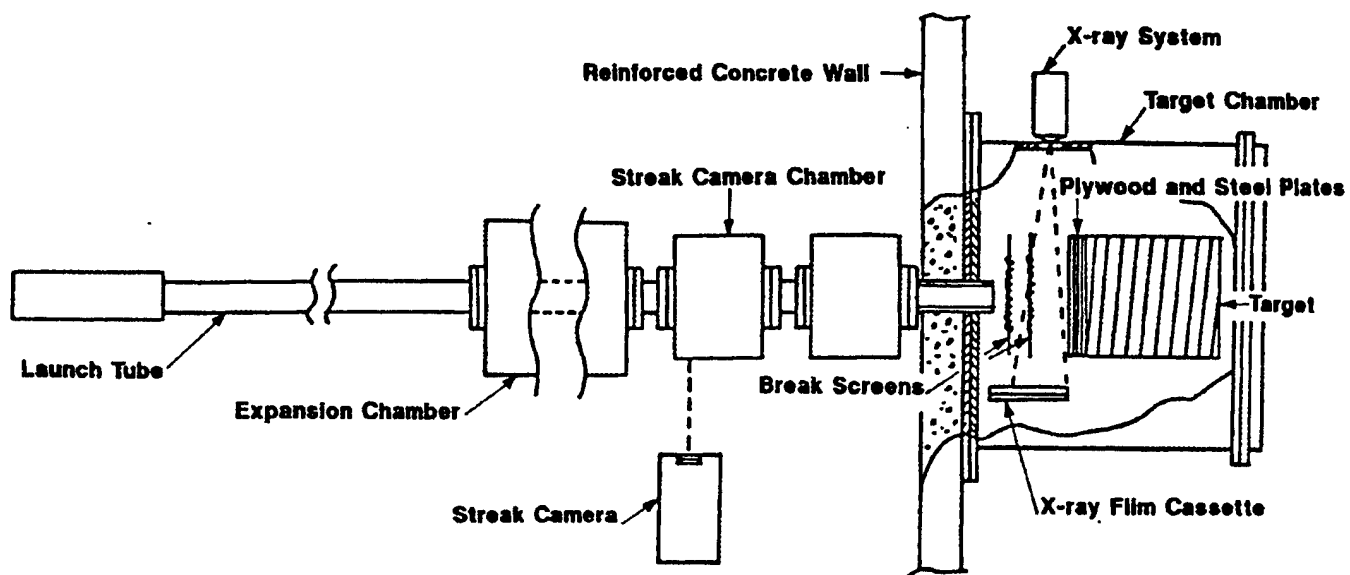
Engineering analysis for a concrete/steel/concrete "composite" is presented in figure 10. The calculations show virtually a linear decrease in the penetration  $P$  with increases in the thickness of the steel layer  $h = z_2 - z_1$ , while the areal weight of the structure  $w = \rho_1 z_1 + \rho_2 h + \rho_3 (P - z_2)$  required to defeat the projectile remains almost the same. Areal cost of this structure was calculated as  $\Omega = \Omega_c (P - h) + \Omega_r h$ , where  $\Omega_c = 0.76 \text{ dollars/m}^2\text{cm}$  and  $\Omega_r = 17.44 \text{ dollars/m}^2\text{cm}$  are the areal costs per unit depth of the structure for the concrete and the reinforcing steel, respectively. The cost of concrete was taken from reference 25 and the  $\Omega_r$  was estimated for the grade 60 no. 4 reinforcing bar from reference 26.

The results of the penetration calculations for a concrete/steel/concrete "composite" for different thickness' of the steel layer as a function of the impact velocity are presented in figure 11. These calculations are compared with similar analysis conducted for plain concrete and plain steel targets. With increases in the thickness of the steel layer, the curves for a "composite" target gradually transition from that of a plain concrete target to that of a plain steel target. The analysis indicates that the penetration performance against a "composite" target is maximized for velocities in the range from  $0.1 \text{ cm}/\mu\text{s}$  to  $0.14 \text{ cm}/\mu\text{s}$ , while the optimum penetration velocities gradually increase as the thickness of the steel layer increases. At lower velocities there exists an additional target failure mode and the application of this model is not expected to be valid. The portions of the curves in this lower velocity region are shown by dotted lines. The unrealistic results obtained for this region are attributed to the qualitatively different mechanism of penetration at lower velocities, where a projectile is able to penetrate the composite target not only by erosion combined with the rigid body motion, but, in addition, by shear plugging of a steel layer of moderate thickness.



## CONCLUSIONS

Spherical-nose copper and tantalum projectiles were launched against concrete and simulant reinforced concrete targets with velocities from 0.15 cm/ $\mu$ s to 0.19 cm/ $\mu$ s. Since the experiments showed that in this velocity range concrete penetration is accomplished by substantial penetrator erosion, a modified hydrodynamic theory of penetration was applied for the analysis of the penetrator motion and for prediction of penetration depths. Comparison between the calculations and various experimental data gave us the following values of the empirical constants appearing in this theory: concrete target strength factor  $R = 4.26$  Kbar, copper penetrator strength factor  $Y = 6.86$  Kbar, and tantalum penetrator strength factor  $Y = 13.44$  Kbar. Using this theory and adopting a rationale for treating reinforced concrete targets as comprised of layers of the concrete proper and reinforcing steel, the penetration resistance of various concrete structures can be estimated very quickly. The method suggested in this work is valid for all but low range of ballistic velocities, that is in the range where the target penetration is accomplished by significant projectile erosion.



(Steel tank containing the target is located behind reinforced concrete wall.)

Figure 1  
Schematic of experimental setup

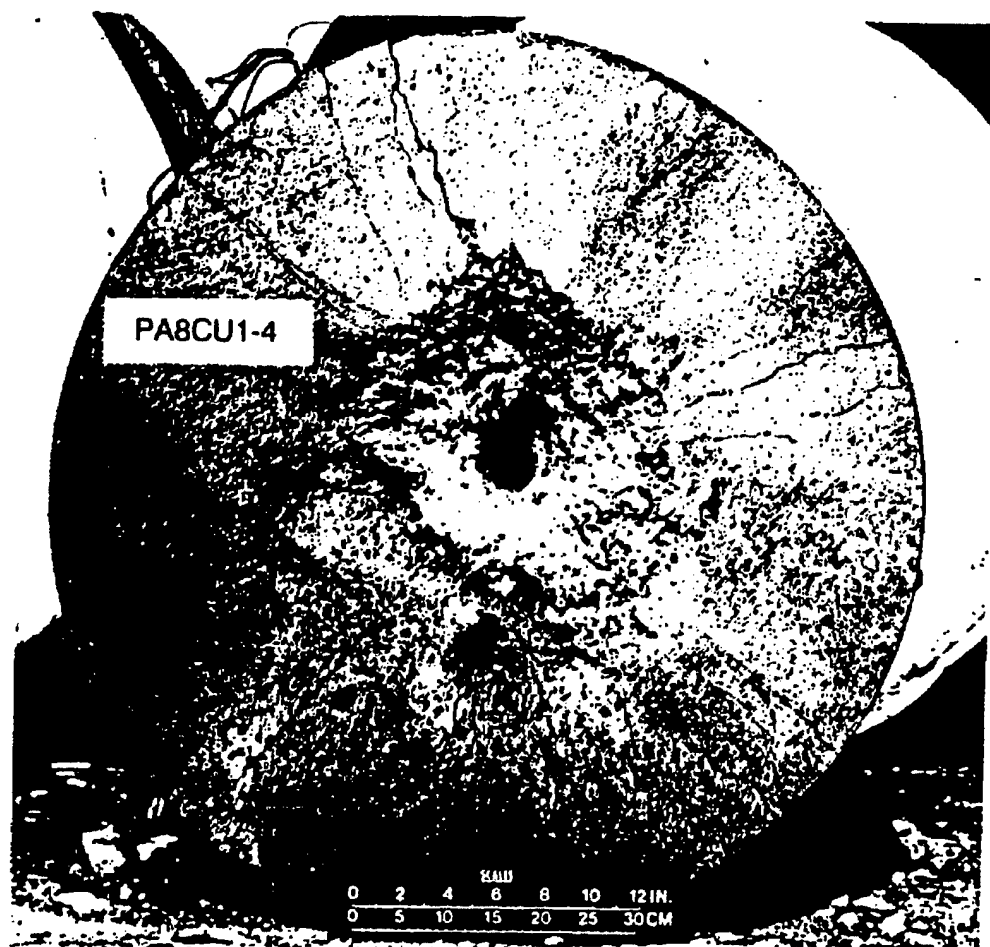
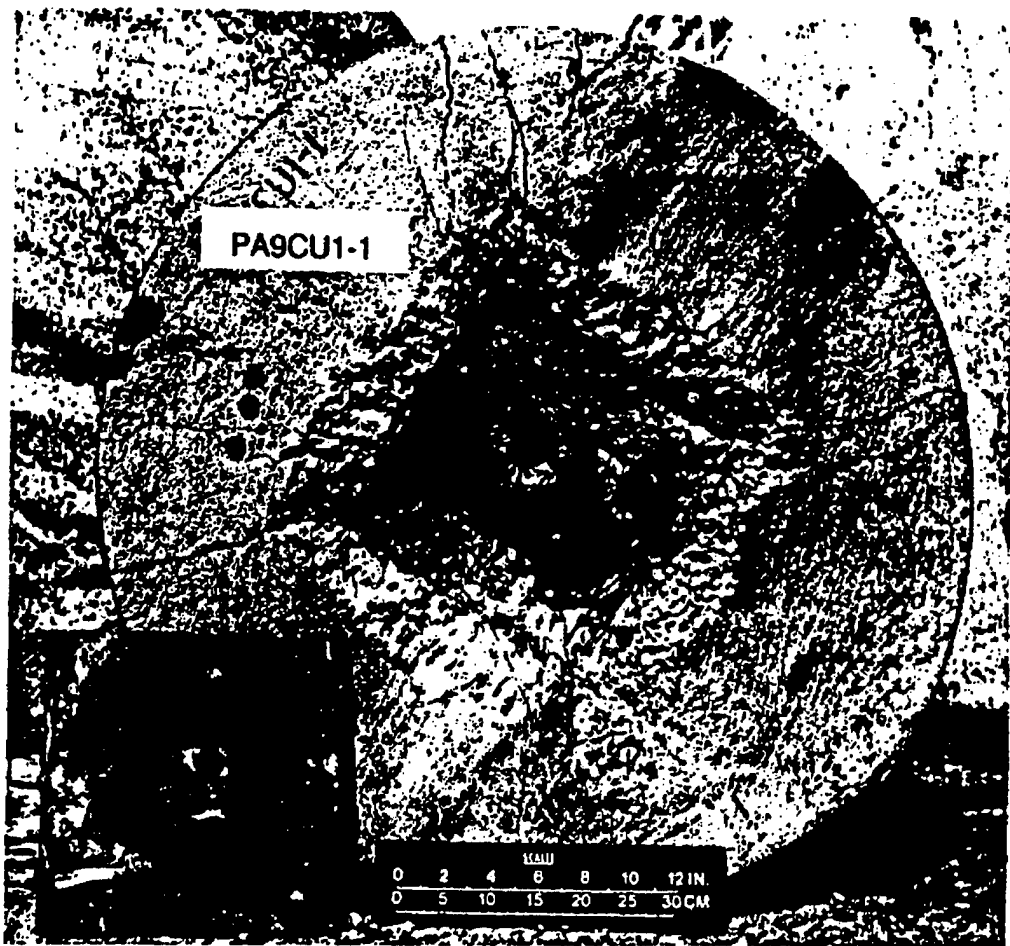


Figure 2  
Plain concrete target after impact



(The welds holding the 30.5-cm square plate failed, and the plate was thrown out from the target.)

Figure 3  
Simulant reinforced concrete target after impact

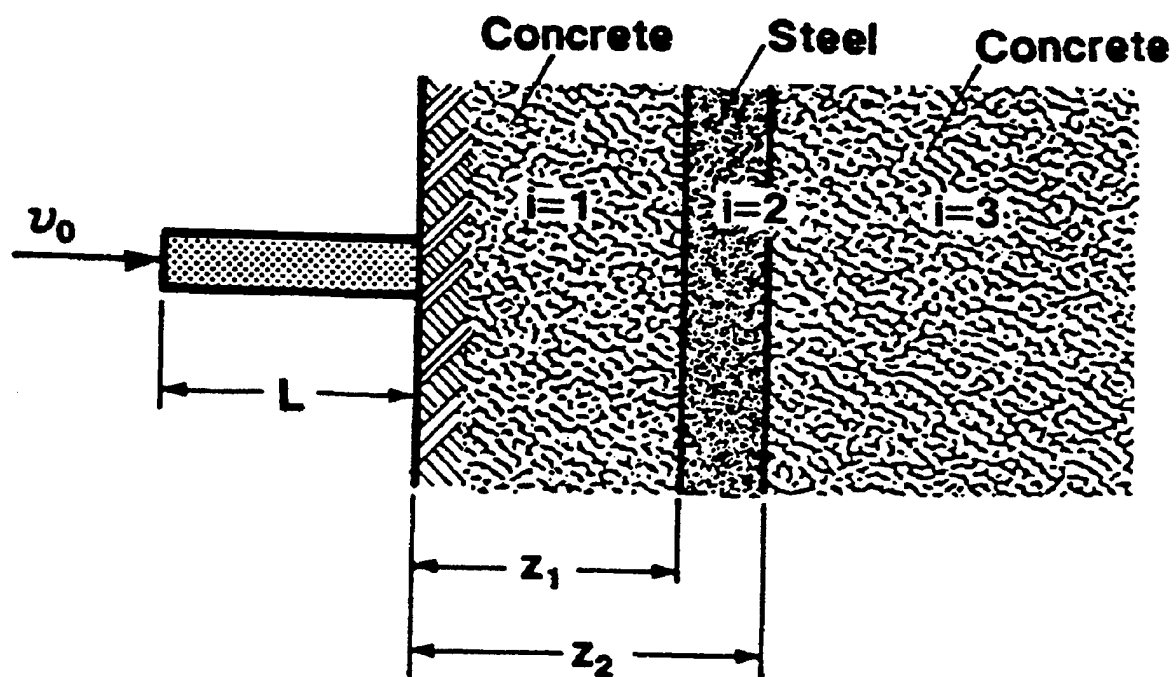


Figure 4  
Rod with initial velocity  $v_0$  impacts  
a composite semi-infinite targets

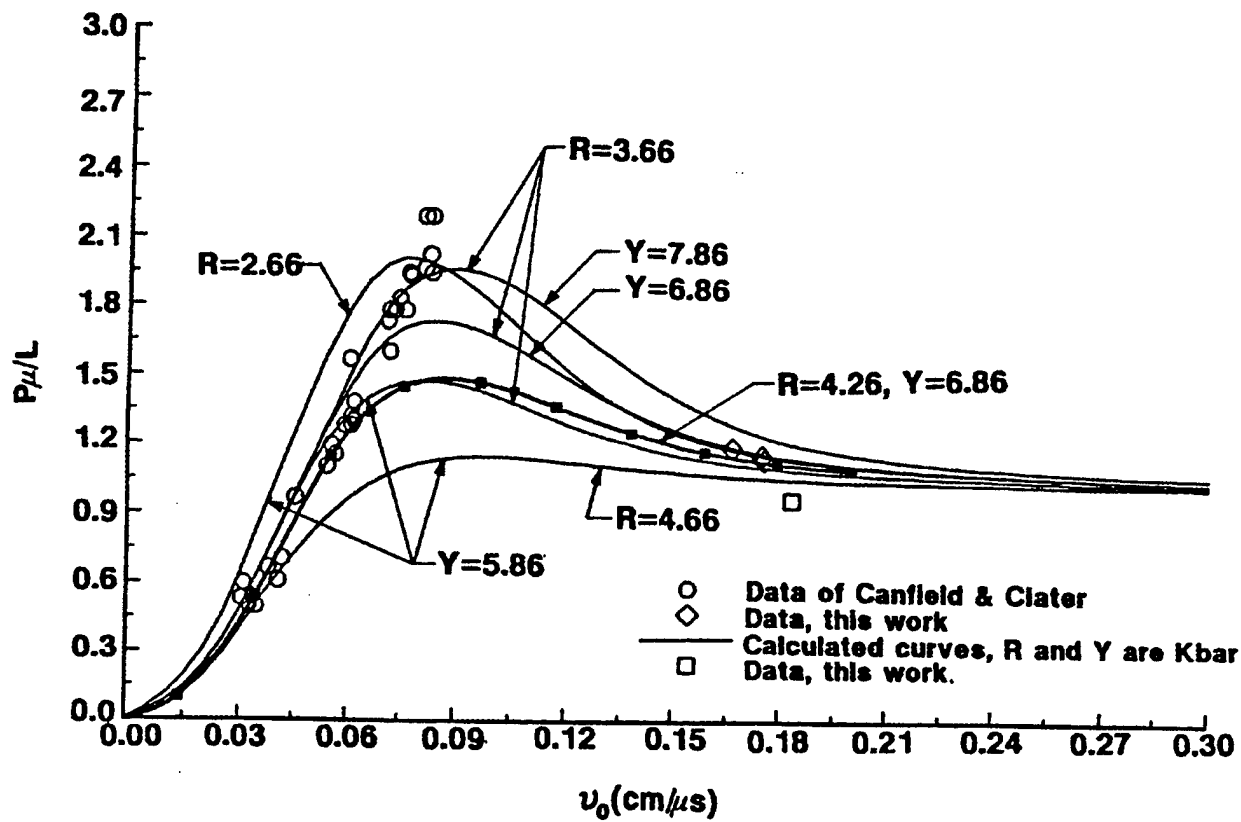


Figure 5  
Normalized penetration depth vs impact velocities

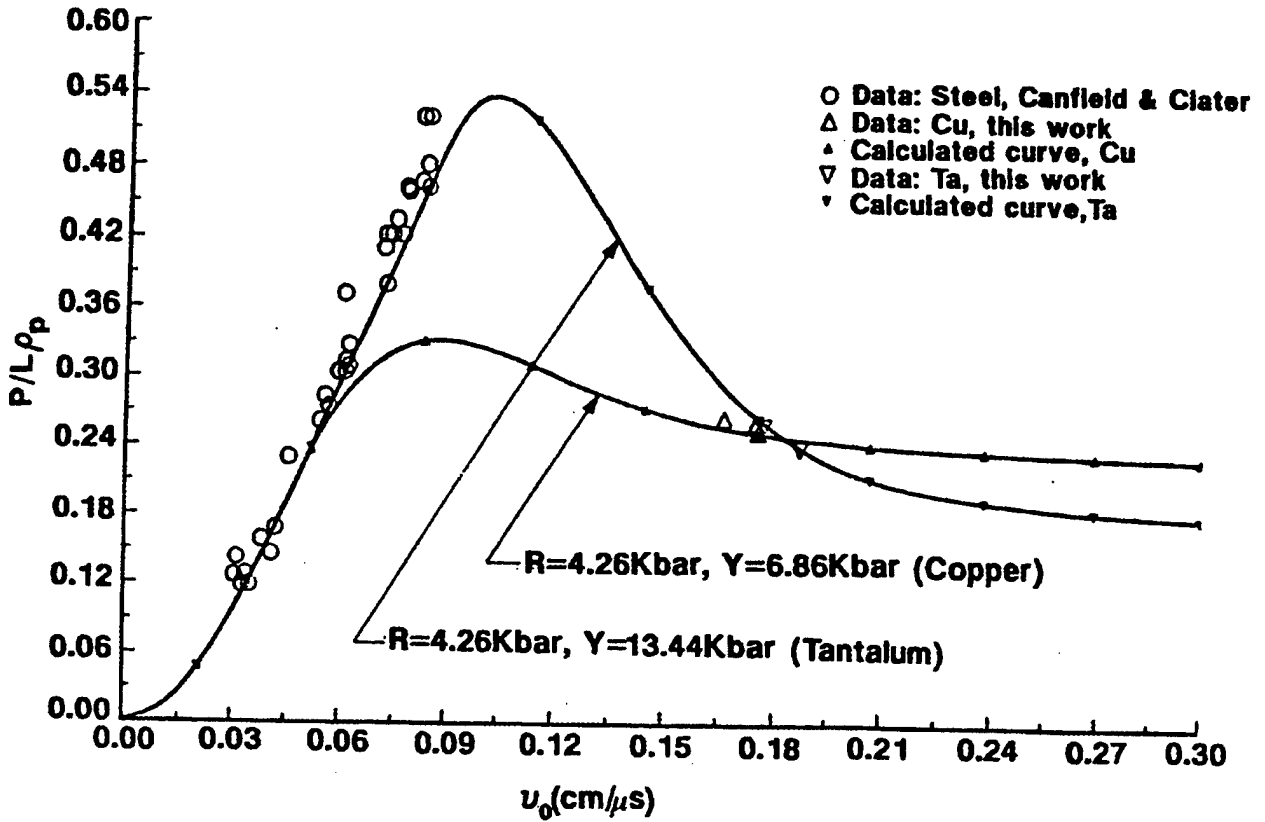
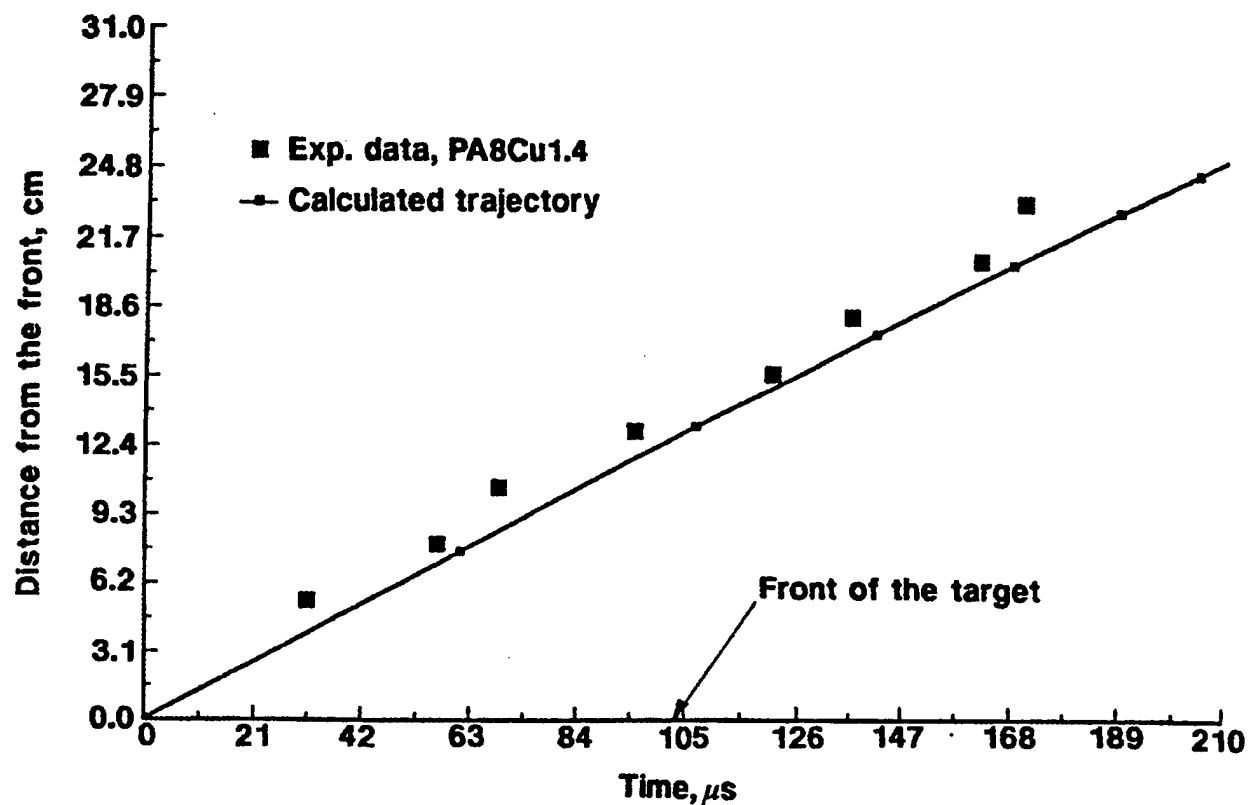


Figure 6  
Calculated penetration performance of copper and tantalum  
projectiles against plain concrete targets compared with  
experimental data for varying impact velocities



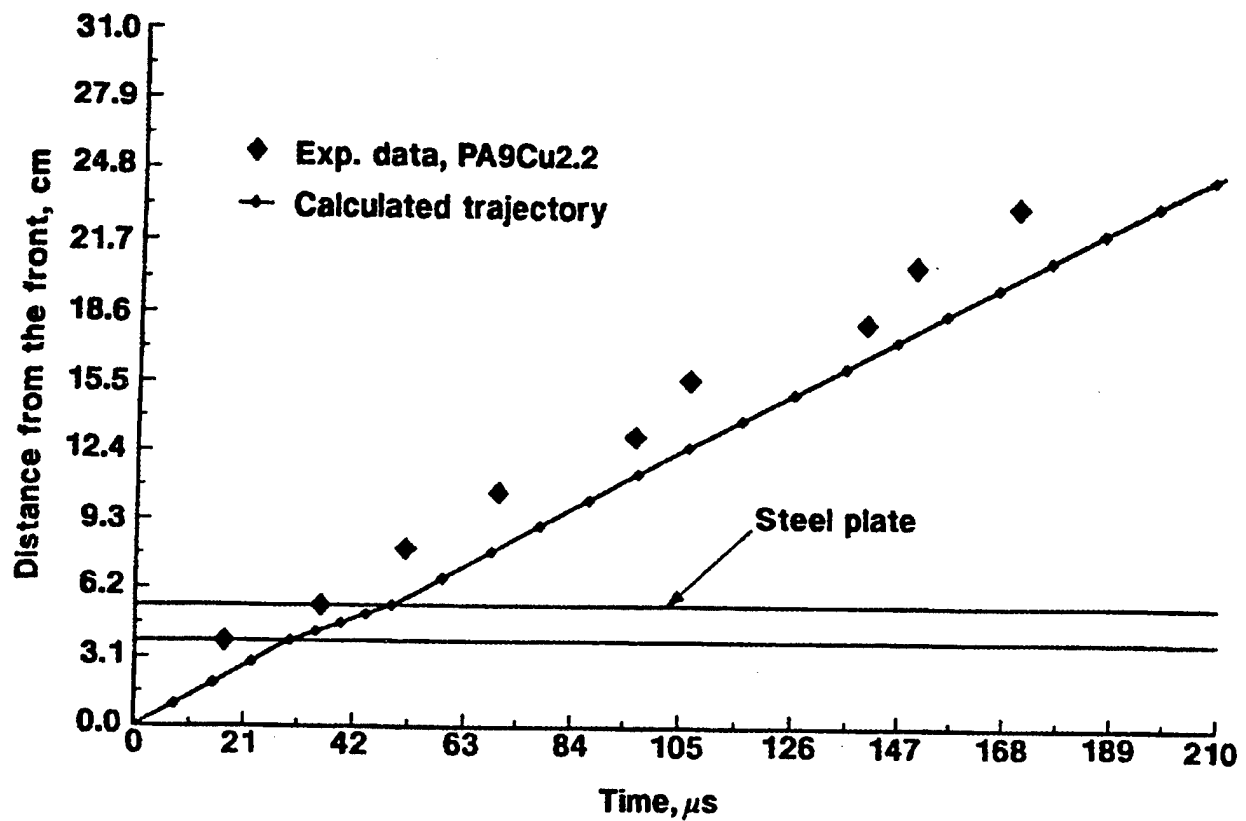
(Parameters used:

$\rho_p = 8.9 \text{ g/cm}^3$ ,  $Y = 6.86 \text{ Kbar}$  for projectile

$\rho_{t1} = \rho_{t3} = 2.24 \text{ g/cm}^3$ ,  $R_{t1} = R_{t3} = 4.26 \text{ Kbar}$  for concrete)

Figure 7  
Calculated trajectories of front end of projectile compared  
with experimental records from break gages - plain  
concrete target,  $v_0 = 0.1836 \text{ cm}/\mu s$



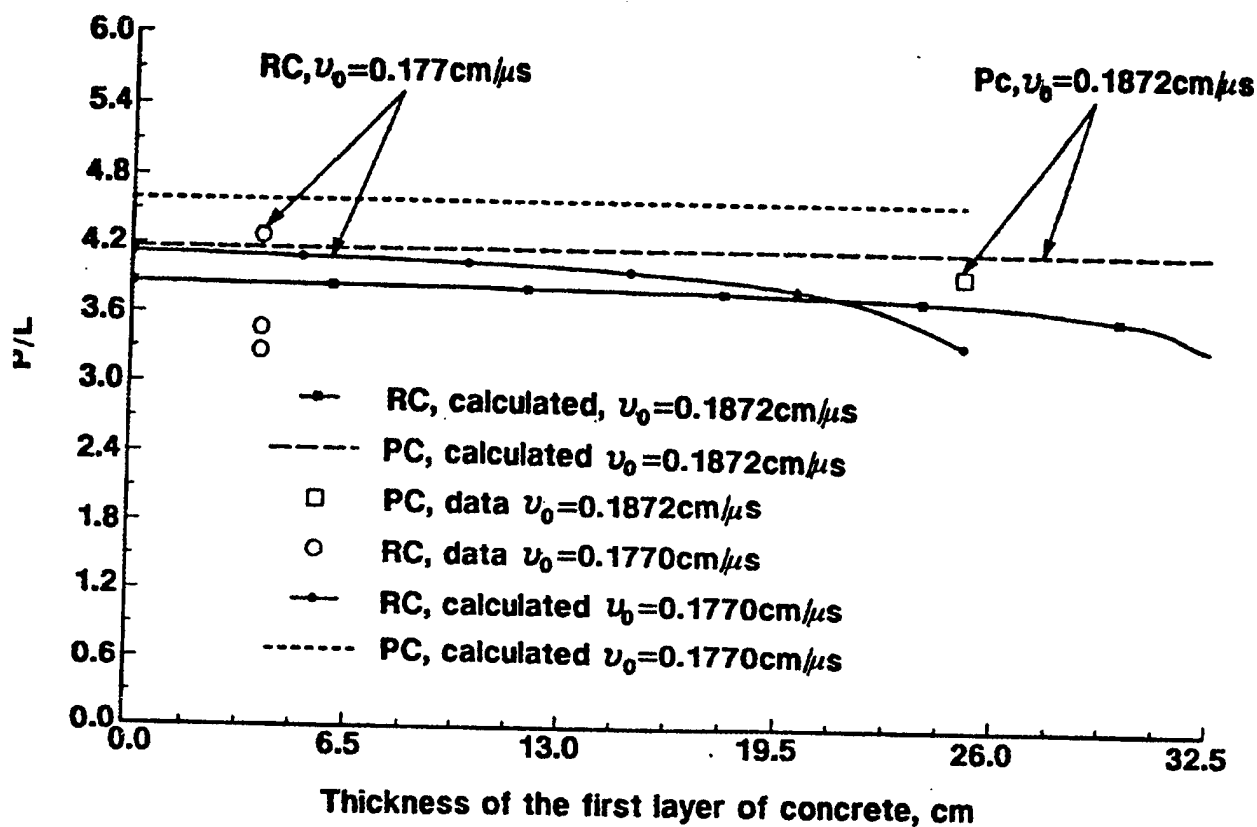


(Parameters used:

$\rho_2 = 7.9 \text{ g/cm}^3$ ,

$R_{t2} = R_{t2} = 26.7 \text{ Kbar}$ ,  $z_1 = 3.81 \text{ cm}$ ,  $z_2 = 5.4 \text{ cm}$  for steel)

Figure 8  
Calculated trajectories of front end of projectiles compared  
with experimental records from break gages - simulant  
reinforced concrete,  $v_0 = 0.1875 \text{ cm}/\mu\text{s}$



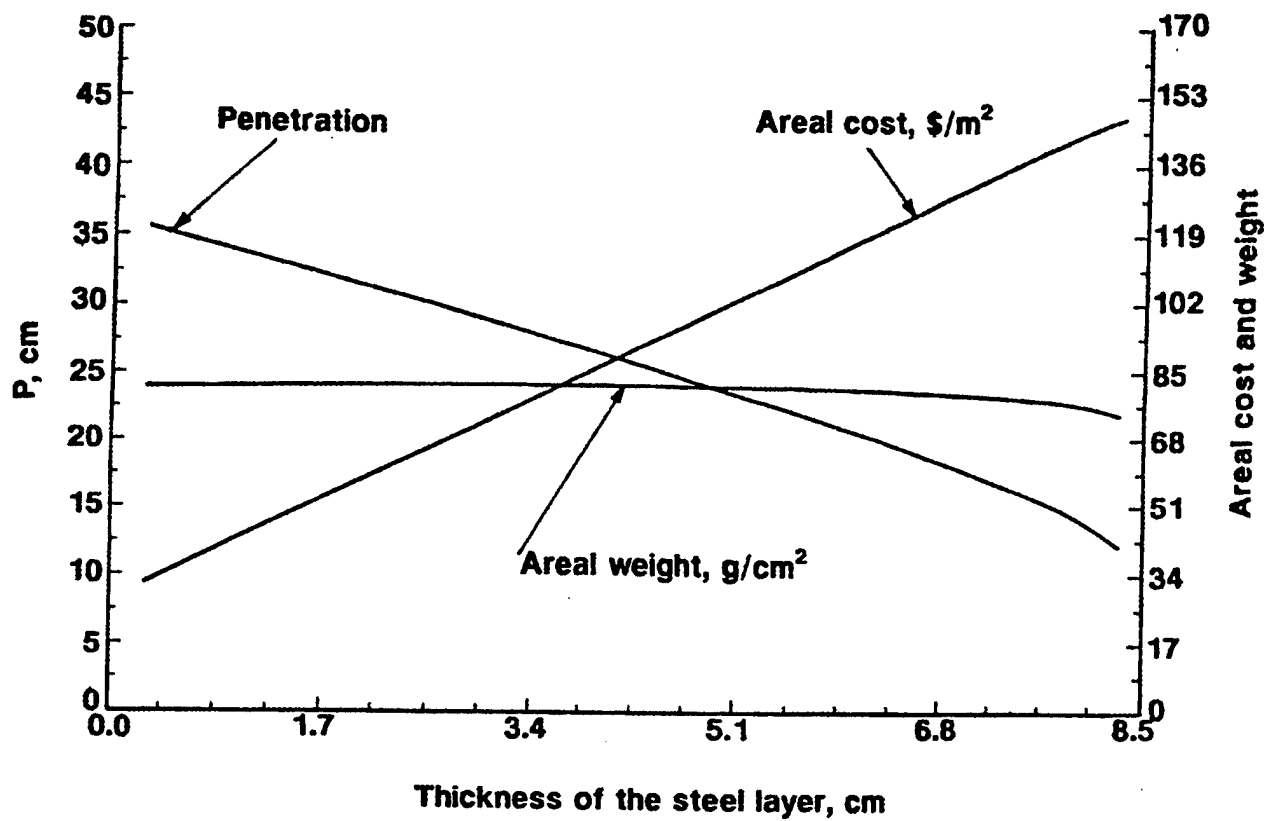
(Parameters used:

$\rho_p = 16.6 \text{ g/cm}^3$ ,  $Y = 13.44 \text{ Kbar}$  for projectile

$\rho_2 = 7.9 \text{ g/cm}^3$ ,  $R_{12} = 26.7 \text{ Kbar}$ ,  $h = z_2 - z_1 = 1.59 \text{ cm}$   
for steel

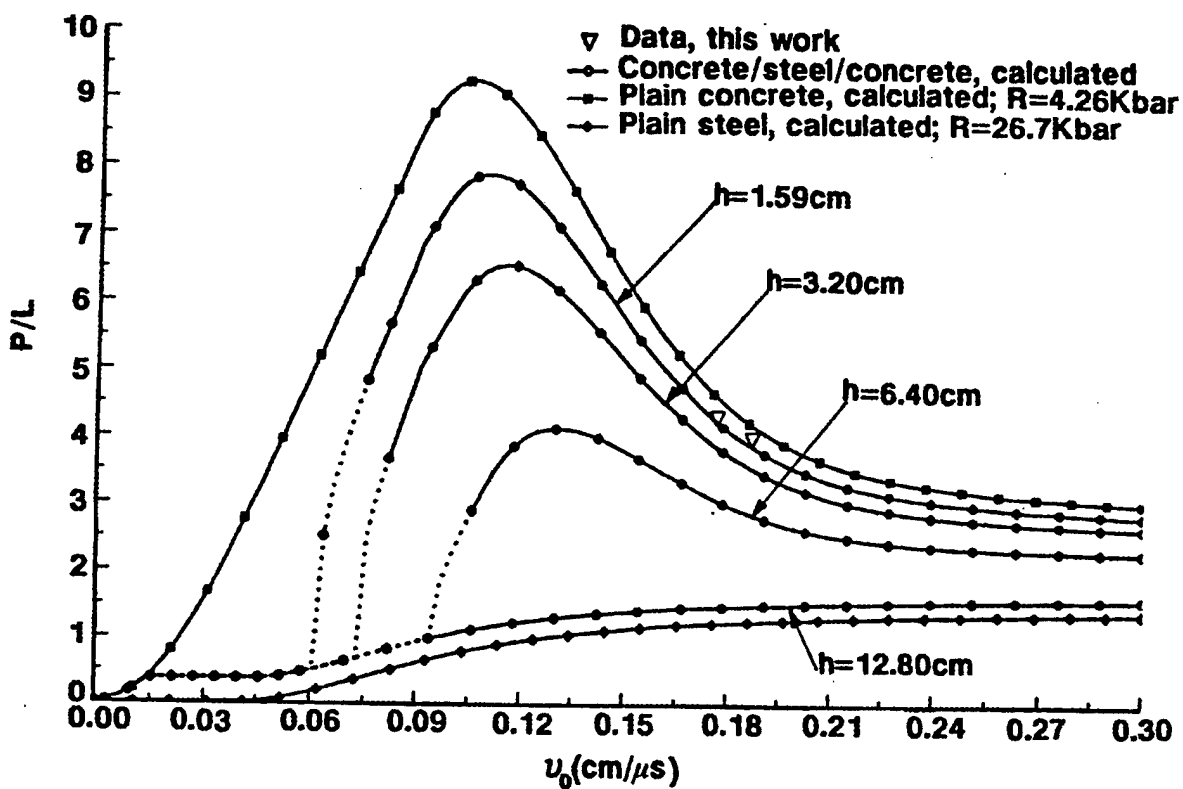
$\rho_1 = \rho_3 = 2.24 \text{ g/cm}^3$ ,  $R_{11} = t_3 = 4.26 \text{ Kbar}$   
for concrete.)

Figure 9  
Resistance of a concrete/steel/concrete composite vs the  
thickness of the surface layer of concrete



(The structure is attacked by a 7.9-cm long tantalum projectile with velocity 0.177 cm/ $\mu$ s.)

Figure 10  
Penetration resistance, areal weight, and areal cost of a concrete/steel/concrete composite structure vs the thickness of the steel layer



(Parameters used:  
 $\rho_p = 16.6 \text{ g/cm}^3$ ,  $Y = 13.44 \text{ Kbar}$  for projectile  
 $\rho_2 = 7.9 \text{ g/cm}^3$ ,  $R_{t2} = 26.7 \text{ Kbar}$  for steel  
 $\rho_{t1} = \rho_3 = 2.24 \text{ g/cm}^3$ ,  $R_{t1} = t_3 = 4.26 \text{ Kbar}$   
 for concrete.)

Figure 11  
 Penetration performance of a tantalum projectile against a concrete/  
 steel/concrete composite with different thickness' of  
 the steel layer vs the impact velocity

Table 1  
Performance of copper (Cu) and tantalum (Ta) projectiles against plain  
concrete targets (PC) and simulant reinforced concrete targets (RC)

Test	Target	Projectile			Impact Velocity cm/ $\mu$ s	Depth of penetration, cm	Projectile mass debris/initial, g
		mat.	diam., cm	length, cm			
PA9Cu1.1	RCi	Cu	1.30	19.00	0.1626	32.5	⊗/224
PA9Cu2.2	RCi	Cu	1.30	14.00	0.1875	25.0	55/164
PA9Ta1.3	RCi	Ta	1.27	10.32	0.1717	35.4	8/216
PA8Cu1.4	PCi	Cu	1.30	19.00	0.1836	36.3	124/224
PA9Cu3.5	RCi	Cu	2.00	14.00	0.1663	33.5	160/381
PA9Ta2.6	RCi	Ta	1.30	7.66	0.1475	25.0	⊗/158
PA9Ta3.7	RCi	Ta	2.00	7.90	0.1770	33.8	⊗/397
PA8Ta1.8	PCi	Ta	1.27	10.32	0.1872	40.9	⊗/215
PA0Cu2.RS9	RC	Cu	1.30	14.00	0.1756	31.5	25/164
PA0Cu2.RL10	RC	Cu	1.30	14.00	0.1750	32.5	⊗/164

(The targets "i" were instrumented with break gages.  
The tests marked "⊗" no projectile debris was reported  
to be found from the sectioning of the targets.)

Table 2  
Hole profiles of tunnel portions of craters\*

Probe Diameter, cm	Depth of the probe, cm						
	PA9Cu1.1	PA9Cu2.2	PA9Ta1.3	PA8Cu1.4	PA9Cu3.5	PA9Ta2.6	PA8Ta1.8
2.0	32.3	23.6	34.5	32.0	26.7	25.0	40.4
2.5	32.1	23.0	32.0	31.5	26.9	25.0	40.4
3.0	32.0	22.2	30.2	31.3	26.5	24.5	39.7
3.5	19.8	17.1	26.2	29.6	26.5	22.9	32.8
4.0	16.6	11.7	18.5	15.2	25.3	19.0	27.9
4.5	15.5	10.0	16.0	12.7	25.2	16.4	26.4
5.0	14.5	9.1	15.0	10.5	25.2	14.8	23.5

\*The measurements were obtained by inserting cylindrical  
gage probes into the hole and measuring the depth from the  
level of the original surface.

## REFERENCES

1. Nash, P.T.; Blaylock N.W.; Spires, S.M.; and Westine, P.S., "Concrete Penetration Data Base and Evaluation of Predictive Equations," SwRI Report No. 06-8691-001, Southwest Research Institute, San Antonio, TX, 1986.
2. Nash, P.T.; Zabel, P.H.; and Wenzel, A.B., "Penetration Studies into Concrete and Granite," Response of Geologic Materials to Blast Loading and Impact, Cizec, J.C. (ed.), ASME/ASCE Mechanics Conference, Albuquerque, NM, AMD-Vol. 69, pp. 175-181, 1985.
3. Canfield, J.A. and Clator, I.G., "Development of a Scaling Law and Techniques to Investigate Penetration in Concrete," NWL Report No. 2057, U.S. Naval Weapons Laboratory, VA, 1966.
4. Cargile, J.D. and Tidwell, L.E., "Penetration of a Subscale Semi-Armor-Piercing Projectile into Conventional-Strength and High-Strength Concrete Targets," WES Report No. SL-93-2, U.S. Army Corps of Engineers, Waterways Experimental Station, Vicksburg, MS, 1993.
5. Forrestal, M.J.; Altman, B.S.; Cargile, J.D.; and Hanchak, S.J., "An Empirical Equation for Penetration of Ogive-Nose Projectiles into Concrete Targets," Int. J. Impact Engineering, Vol. 15, pp. 395-405, 1994.
6. Haldar, A. and Miller, F.J., "Penetration Depth in Concrete for Nondeformable Missiles," Nuclear Engineering Design, Vol. 71, pp. 79-88, 1982.
7. Hughes, G., "Hard Missile Impact on Reinforced Concrete," Nuclear Engineering Design, Vol. 77, pp. 23-35, 1984.
8. Riera, J.D., "Penetration, Scabbing and Perforation of Concrete Structures Hit by Solid Missiles," Nuclear Engineering Design, Vol. 115, pp. 121-131, 1989.
9. Forrestal, M.J.; Norwood, F.R.; and Longcope, D.P., "Penetration into Targets Described by Locked Hydrostats and Shear Strength," Int. J. Solids Structures, Vol. 17, pp. 915-924, 1981.
10. Forrestal, M.J.; Luk, V.K.; and Watts, H.A., "Penetration of Reinforced Concrete with Ogive-Nose Penetrators," Int. J. Impact Engineering, Vol. 24, pp. 77-87, 1988.
11. Krause, D.R.; Wuerer, J.E.; and Oedling, R.G., "Ballistic Range/Guided Rail Track Test Conductor Program Interim Report, Volume II, Impact Technology Tests," SDL Report No. 82-2100-173, Spectron Development Laboratories, Inc., CA, 1981.

## REFERENCES (cont)

12. Orphal, D.L.; Miller, C.W.; McKay, W.L.; Borden, W.F.; Larson, S.A.; and Kennedy, C.M., "Hypervelocity Impact and Penetration of Concrete by High L/D Projectiles," ADPA, Proceedings of the Seventh Ballistics Symposium, 1982.
13. Birkhoff, G.; MacDougal, D.P.; Pugh, E.M.; and Sir Taylor, G., "Explosives with Lined Cavities," J. Appl. Phys., Vol. 19, pp. 563-582, 1948.
14. Miller, C.W. and McKay, W.L., "Perforation of Concrete Targets by Slender Metal Rods," ADPA, Proceedings of the Sixth Ballistics Symposium, pp. 502-509, Orlando, FL, 1981.
15. Alekseevskii, V.P., "Penetration of a Rod into a Target at High Velocity," Combustion, Explosion and Shock Waves, Vol. 2, pp. 63-66 (translated from the Russian), Farady Press, NY., 1966.
16. Tate, A., "A Theory for Deceleration of Long Rods After Impact," J. Mech. Phys Solids, Vol. 15, pp. 387-399, 1967.
17. Eichelberger, R.L., "Experimental Test of the Theory of Penetration by Metallic Jets," J. Appl. Phys., Vol. 27, pp. 63-68, 1956.
18. Allen, W.A.; Mayfield, E.B; and Morrison, H.L., "Dynamics of a Projectile Penetrating Sands," J. Appl. Phys., Vol. 28., pp. 370-376, 1957.
19. Weihrauch, G., "The Behavior of Copper Pins Impacting Different Materials at Speeds between 50 m/s and 1650 m/s," ISL Report No. 7/71, Franco-German Research Institute, Saint Louis, France, 1971.
20. Lehr, H.F. and Weihrauch, G., "Target Deformation in Front of a Hydrodynamically Penetrating Rod Projectile," Technical Report No. 14/73, Franco-German Research Institute, Saint France, 1973.
21. Netherwood, P.H., Jr., "Rate of Penetration Measurements," BRL Memorandum Report No. ARBRL-MR-02978, Ballistic Research Laboratory, Aberdeen Proving Ground, MD, 1979.
22. Tate, A., "Further Results in the Theory of Long Rod Penetration," J. Mech. Phys. Solids, Vol. 17, pp.141-150, 1969.
23. Anderson, C.E. Jr. and Bodner, S.R., "Ballistic Impact: the Status of Analytical and Numerical Modeling," Int. J. Impact Engineering, Vol. 7, pp. 9-35, 1988.

**REFERENCES**  
**(cont)**

24. Wilkins, M.L. and Guinan, M.W., "Impact of Cylinders on a Rigid Boundary," J. Appl. Phys., Vol. 44, No. 3, pp. 1200-1206, 1973.
25. Material Prices, Engineering News Record, p. 41, June 1, 1992.
26. Material Prices, Engineering News Record, p. 159, June 22, 1992.



## DISTRIBUTION LIST

Commander  
Armament Research, Development and Engineering Center  
U.S. Army Tank-automotive and Armaments Command  
ATTN: AMSTA-AR-LSL (2)  
AMSTA-AR-GCL  
AMSTA-AR-AEE  
AMSTA-AR-AAE-W (3)  
Picatinny Arsenal, NJ 07806-5000

Defense Technical Information Center (DTIC)  
ATTN: Accession Division (12)  
8725 John J. Kingman Road, Suite 0944  
Fort Belvoir, VA 22060-6218

Director  
U.S. Army Materiel Systems Analysis Activity  
ATTN: AMXSY-EI  
392 Hopkins Road  
Aberdeen Proving Ground, MD 21010-5423

Commander  
Chemical/Biological Defense Agency  
U.S. Army Armament, Munitions and Chemical Command  
ATTN: AMSCB-CII, Library  
Aberdeen Proving Ground, MD 21010-5423

Director  
U.S. Army Edgewood Research, Development and Engineering Center  
ATTN: SCVRD-RTB (Aerodynamics Technology Team)  
Aberdeen Proving Ground, MD 21010-5423

Director  
U.S. Army Research Laboratory  
ATTN: AMSRL-OP-CI-B, Technical Library  
Aberdeen Proving Ground, MD 21005-5066

Chief  
Benet Weapons Laboratory, CCAC  
Armament Research, Development and Engineering Center  
U.S. Army Tank-automotive and Armaments Command  
ATTN: AMSTA-AR-CCB-TL  
Watervliet, NY 12189-5000

**DISTRIBUTION LIST**  
**(cont)**

Director  
U.S. Army TRADOC Analysis Command - WSMR  
ATTN: ATRC-WSS-R  
White Sands Missile Range, NM 88002

Commander  
Naval Air Warfare Center Weapons Division  
1 Administration Circle  
ATTN: Code 473C1D, Carolyn Dettling (2)  
China Lake, CA 93555-6001

GIDEP Operations Center  
P.O. Box 8000  
Corona, VA 91718-8000